Applied Medical Informatics
Original Research Vol. 32, No. 1/2013, pp: 33-42

Automatic Detection of Retinal Exudates using a Support Vector Machine

Kittipol WISAENG[1,*], Nualsawat HIRANSAKOLWONG[1], and Ekkarat POTHIRUK[2]

[1] Department of Computer Science, King Mongkut's Institute of Technology Ladkrabang, Bangkok 10520, Thailand.
[2] Ophthalmology Unit, Khonkaen Hospital, Khonkaen 40000, Thailand.
E-mail(*): s3650502@kmitl.ac.th

* Author to whom correspondence should be addressed; Tel.: +66 (0) 2326 4339

Received: 11 January 2013 /Accepted: 18 February 2013 / Published online: 25 February 2013

Abstract
Retinal exudates are among the preliminary signs of diabetic retinopathy, a major cause of vision loss in diabetic patients. Correct and efficient screening of exudates is very expensive in professional time and may cause human error. Nowadays, the digital retinal image is frequently used to follow-up and diagnoses eye diseases. Therefore, the retinal image is crucial and essential for experts to detect exudates. Unfortunately, it is a normal situation that retinal images in Thailand are poor quality images. In this paper, we present a series of experiments on feature selection and exudates classification using the support vector machine classifiers. The retinal images are segmented following key preprocessing steps, i.e., color normalization, contrast enhancement, noise removal and color space selection. On data sets of poor quality images, sensitivity, specificity and accuracy is 94.46%, 89.52% and 92.14%, respectively.

Keywords: Exudates, Diabetic retinopathy, Digital retinal image, Support vector machine

Introduction

Retinal exudates are a sign of a severe eye disease and a major cause of blindness. Exudates need regular screening because early detection of exudates could help patients prevent blindness. However, manual examination by expert ophthalmologists takes time and the number of experts is not sufficient to meet the demand for screening. Given the limitations of manual screening, the prospect of automatic detection of exudates, towards diagnosis and tracking the progress of a patient's treatment program, is enticing.

A large number of techniques for detection of exudates has been published. Zhang et al. [1] used local contrast enhancement and fuzzy c-mean clustering (FCMC) in Luv color space to segment candidate bright exudates areas. However, the main difficulty with FCMC is determining the number of clusters to use. Walter et al. [2] applied mathematical reconstruction to detect contours typical of exudates. This technique achieved predictive and sensitivity values of 92.4% and 92.8% with a set of 15 abnormal retinal images. However, this technique did not discriminate exudates from cotton wool spots. Gardner et al. [3] used the back propagation neural network for the segmentation of exudates. Comparing the results of this method with those of an expert ophthalmologist, the method achieved a sensitivity and specificity of 88.4% and 83.5%, respectively, for the detection of exudates. A drawback of this method was that it did not work well

on poor quality images.

Most of the previous work was based on retinal features with clearly visible on acquired imagery. Since acquiring clearly visible retinal features takes time and is uncomfortable for patients, this paper proposes methods for automated detection of exudates on imagery with poor quality retinal images. The ultimate aim was to develop an application for automatic detection of exudates, to provide decision support and reduce workloads for expert ophthalmologists'.

Material and Method

We acquired 120 digital retinal images taken from a screening program for diabetic retinopathy in Mahasarakham Hospital, Thailand. The images were captured in 24-bit color with a KOWA-7 non-mydriatic retina camera with 45º field of view. We scaled all images to 700 × 500 pixels.

First, the raw images were processed method, such as color normalization, contrast enhancement, noise removal and color space selection of the image. We then eliminated the optic disc and extracted the features in a retinal image in a retinal image. Our feature selection and classification experiments with the support vector machine classifiers were used to describe the method and measure the application's performance. The overall procedure of the clinical application is shown in Figure 1.

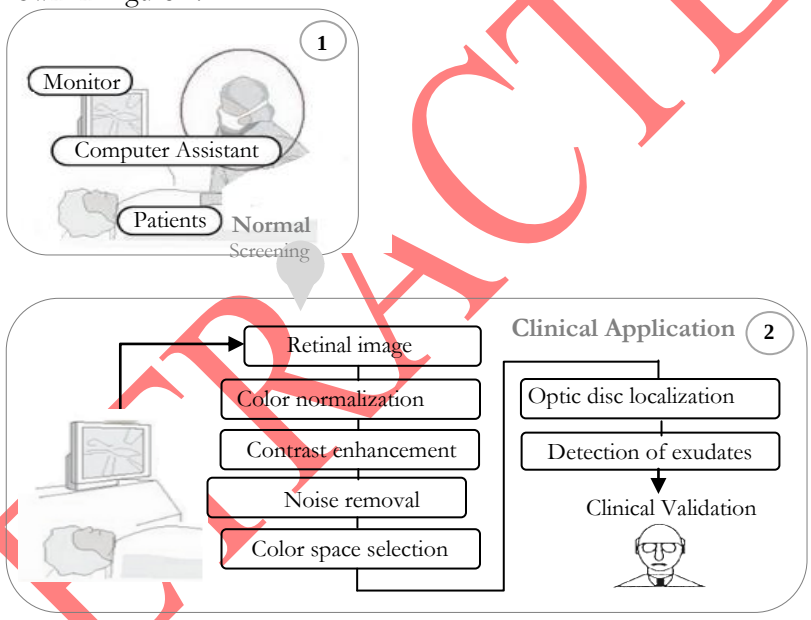

Figure 1. The outline of the proposed system for automatic detection of exudates

To obtain an image suitable for feature selection, we put our retinal image data through four preprocessing steps before commencing the detection of exudates.

Color Normalization

Color normalization does not aim to find the true object color, but to transform the color to be invariant with changes in the illumination -without losing the ability to differentiate between the objects of interest.

Three normalization techniques were tested on a set of retinal images (grey-world normalization [4], histogram equalization [5], and histogram specification [6]). Color classification is intended to improve overall classification accuracy. Histogram specification was found to be the most effective normalization method, improving the clustering of the different lesion types, removing at least some of the variation due to retinal pigmentation differences between individuals. Thus, we selected a retinal image as a reference (Figure 2(**a**)) and applied the described histogram specification technique to modify the values of each image in the data set such that its frequency

histogram matched the reference image distribution. The histogram specification technique was independently applied to each individual RGB channel to match the shapes of three specific histograms of the reference image. Here, the reference histograms were taken from an image, which represents a frequent retinal pigmentation color among our image dataset (the effect of histogram specification is shown in Figure 2(**b**)).

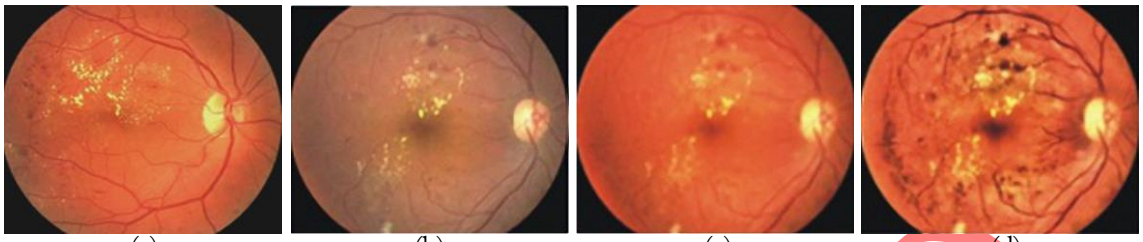

(a) (b) (c) (d)

Figure 2 Color normalization and local contrast enhancement. (**a**) Reference image. (**b**) Typical abnormal image. (**c**) Color normalized version of (**b**). (**d**) After contrast enhancement.

Contrast Enhancement

As seen in the previous section, quality of retinal image has a great impact on the features of exudates. However, the contrast decreases with the distance of pixels from the center, especially in the periphery. We applied local contrast enhancement [7] to distribute the values of pixels around the local mean. If the variation of the intensity in the local area is high, the algorithm does not significantly increase the local contrast. On the other hand, if the intensity variation in the local area is small, the local contrast is substantially increased.

Noise Removal

While the contrast enhancement improves the contrast of exudates, it may also enhance the contrast of some non-exudates background pixels (e.g., noise or artifact), these pixels can wrongly be identified as exudates. Here, after to contrast enhancement, there are several ways to remove or reduce noise in an image such as linear filtering, adaptive filtering and median filtering. The median filter replaces the value of a pixel by the median of the gray levels in the neighborhood pixels. The median filter is much less sensitive than the mean to outliers. Median filtering is better able to remove these outliers without reducing the sharpness of the image. The benefit of median filter is simultaneously reducing noise (notably shot noise or salt and pepper noise) and preserving edges. Therefore, a median filtering operation was applied in this step.

Color Space Selection

Color retinal images contain more information about objects and background than the corresponding grey level images. Thus, the first task in color image processing is to choose an appropriate representation using a color space definition. There are several different color spaces in literature [8] and each has its own advantages. The selection of a color space for image processing is application dependent. Indeed; there is no one-color space that is better than the others and suitable for all kinds of images.

To select the most suitable color space for our classification approach, we conducted a quantitative analysis and utilized the evaluation function value J = trace (S_b/S_w) as a measure of color space efficiency [9]. This function estimates the class separate of our exudates and non-exudates pixels classes in different color spaces and was measured using within-class and between classes scatter matrices. The within-class scatter matrix (S_w) indicates the distribution of sample points around their respective mean vectors and (S_b) represents the scatter of samples around the mean vector of class mixture. In fact the numerator of function J represents the overall color difference of exudates and non-exudates sample points, while the denominator denotes the variations of the color distribution for these two classes. A higher value of J shows that the classes are more separated, while the numbers within each class are closer to each other. We have

experimented with various color spaces such as RGB, YIQ, HIS, HSL, Lab and Luv color space, Luv color space [6] appeared to be the most appropriate space for our segmentation. Therefore, RGB space from the third preprocessing step was transformed to Luv space.

Optic Disc Localization

Optic disc (OD) localization is necessary as a prerequisite stage in algorithms applied for detection of retinal anatomical structures and lesions. The OD is indispensable in our automatic detection of exudates, since it illustrates similar attributes to the exudates in terms of color, brightness and contrast. Despite its importance, an accurate localization is not an easy task, as some parts of the boundary are not well defined in some images and several parts are obscured by the crossing blood vessels. Some of these difficulties, which are experienced in OD localization, are apparent in Figure 3. Sometimes the whole OD is brighter than the surrounding area, therefore the OD can be seen as a disc; or it can appear as a hollow ring. The central portion of disc is the brightest region called optic cup (OC). In either case the cup appears as a smaller, brighter region within the OD. Whereas locating the OD and traceing its boundaries is an apparently simple task for an expert, traditional general-purpose boundary detection algorithms have not fully succeeded in detecting the OD due to fuzzy boundaries or missing edge features. Therefore, a reliable OD localization is surprisingly difficult.

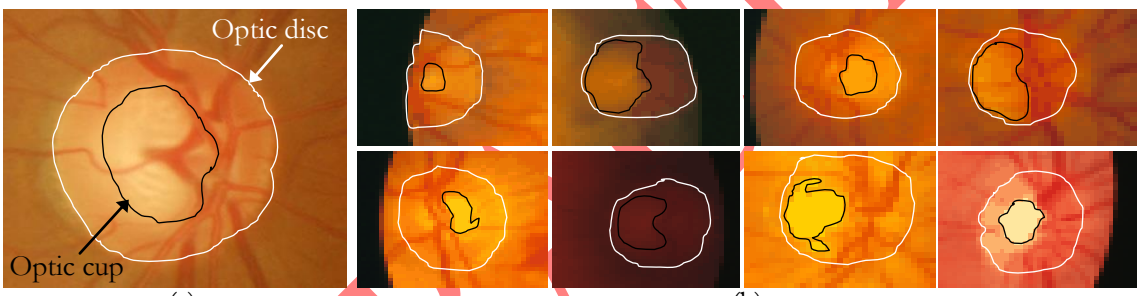

Figure 3 (**a**) OD and OC in retinal image. (**b**) The varying location of OD and OC.

To locate the OD, two techniques are presented in this paper: a combination of morphology methods and Otsu's algorithms. The OD is characterized by the largest high contrast among circular shape areas. While vessels also appear with high contrast, the size of the area is much smaller. Applying a closing operator (f) on the intensity channel (C_I) will help eliminate the vessels which may remain in the OD region. Figure 4(**a**) shows a result after closing operator, Equation (1) was applied.

$$OD = f^{(B_1)}(C_I) \tag{1}$$

where B_1 is the morphological structuring element. The resulting image was binarized by thresholding (α_1), shown in Figure 4(**b**) and the threshold image was then used as a mask. All pixels in the mask were inverted before they overlay on the original image to remove candidate bright regions. The result, OD_2, is shown in Figure 4(**c**). The morphological reconstruction by dilation, R, was then aplied on the prevoiusly overlaid image.

$$OD_3(x) = R_{C_I}(OD_2) \tag{2}$$

The dilations of marker image (OD_2) under mask image (C_I) were repeated until the contour of marker image fitted under the mask image. The reconstructed image is shown in Figure 4(**d**). The difference between the original image and the reconstructed image was thesholded at grey level (α_2) using Equation (3). The value of α_2 is different from image to image depending on automated selection using the Otsu's algorithm.

$$OD_4 = T_{\alpha_2}\left(C_I - OD_3\right) \tag{3}$$

As a result, high intensities are reconstructed while the rest is removed, as shown in Figure 4(**e**). The selected result, OD_5, was dilated with a binary dilation operator (δ) in Equation (4) to ensure that all pixels in the OD area were covered. In this step, a flat disc shaped structuring element with a fixed radius of six (B_2) was used.

$$OD_{seg} = \delta^{(B_2)}\left(OD_5\right) \tag{4}$$

All OD area in the original image was marked out using the previous output. The result is shown in Figure 4(**f**).

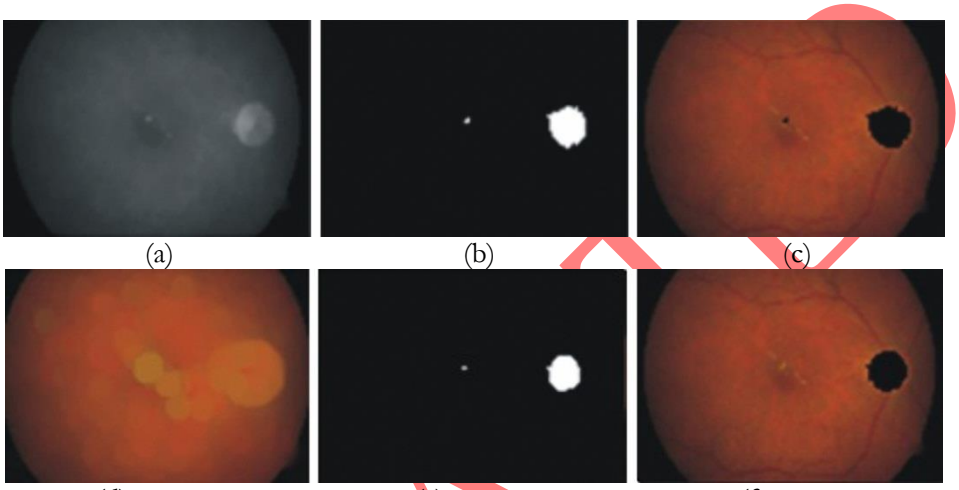

Figure 4 (**a**) Intensity image after closing. (**b**) Thresholded image. (**c**) Marker image. (**d**) Reconstructed image. (**e**) Thresholded result of difference image. (**f**) OD area eliminated

We computed the accuracy of the boundary localization against the manually labeled ground-truth produced by expert ophthalmologists. We used a simple and effective overlap measure of the between two regions:

$$M = \frac{n\left(R \cap T\right)}{n\left(R \cup T\right)} \times 100 \tag{5}$$

where R corresponds to the ground-truth in white, T is the final OD contour region and n(.) is the number of pixels in a region. In the optimal case, when both contours perfectly match M = 100. The measure M represents the accuracy. The proposed method was compared with the hand-labeled ground-truth information from expert ophthalmologists, the local dataset and publicly available datasets were used to test the proposed method.

Feature Selection

Exudates can be identified on an ophthalmoscope as areas with hard yellowish colors. They have varying sizes, shapes, and locations near the leaking capillaries within the retina.

We asked expert ophthalmologists how they identify exudates in an image, so that our feature extraction would reflect expert ophthalmologists' expertise. We found that color, shape and texture are among those top features they look at. To differentiate exudates pixels from non-exudates pixels, we attempted to mimic ophthalmologist expertise by extracting these relevant and significant features. Six features were experimentally selected as input algorithms. Four features from the preprocessing steps and two features from the number of edge pixels and the standard deviation of

preprocssed intensity values in a window around a pixel. We used a window size of 15×15. We used the standard deviation because exudates tend to be more highly textured than non-exudates regions, and the standard deviation is a simple indication of texture. We applied a Sobel edge operator with a mask size of a 17×17 neighborhood to eliminate the strong edges arising from blood vessels and the optic disc.

Knowledge Base Construction

In this section, we introduce a binary classification scheme with the objective of discriminating exudates pixels from non-exudates in an automatic and efficient way. To construct learning datasets of exudates and non-exudates pixels, a consultant ophthalmologist' manually segmented a number of representative retinal images and marked the exudates lesions. An almost balanced learning dataset of exudates and non-exudates was established to eliminate any possible bias towards either of the two classes. Our representative leaning dataset comprised of 71,890 exudates and 65,606 non-exudates pixels. The exudates pixels were collected from 98 manually segmented abnormal images. Similarly, the non-exudates pixels were collected from 22 normal images. Table 1 indicates the exudates and non-exudates sample points used for the cross validation scheme.

Table 1. The number of exudates and non-exudates pixel numbers for training and validation

	Exudates sample	Non-exudates sample points
Training set	50,323	45,924
Validation set	21,567	19,682
Overall	71,890	65,606

Detection of Exudates using Support Vector Machine Classifiers

A support vector machine (SVM)[10] maps training data into a high-dimensional feature space in which we can construct a separating hyperplane maximizing the margin, or distance from the hyperplane to the nearest training data points.

In the put space, a binary support vector machine's decision function can be written:

$$f(x) = \sum_{i \in s} \alpha_i y_i K(x_i, x) + b \qquad (6)$$

where **x** is the feature vector to be classified, **i** indexes the training example, **S** is a set of indices for which $\mathbf{x}_i$ is a support vector, i.e, a vector for which $\boldsymbol{\alpha}_i \neq 0$ after optimization, $\boldsymbol{\alpha}_i$ and **b** are fit to the data to maximize the margin, $\mathbf{y}_i$ is the label [-1, 1] of training example i, and K(.,.) is the kernel function. A serious problem with nonlinear kernel SVM is their complexities of classification which are high when a large number of support vectors is needed.

There are many kernels that can be used, such as linear, polynomial, radial basis function (RBF) and sigmoid. We chose an RBF kernel, because it can handle the case when the relation between class labels and attributes is nonlinear. Furthermore, an RBF kernel has less hyperparameters than a polynomial kernel. The RBF kernel can be written as follows:

$$K(x_i, x_j) = \exp\left(-\frac{\|x_i - x_j\|^2}{2\sigma^2}\right) \qquad (7)$$

where $\sigma > 0$ is a constant that defines the kernel width. We first constructed a set of SVM classifiers with a range of values for the kernel parameter σ and with no restriction on the Lagrange multipliers α_i (i.e. hard margin approach). In this case, the number of RBF centers, the centers or

the support vectors, α_i and b were all automatically obtained by the SVM training procedure. We found that the best generalization accuracy was achieved when $\sigma = 0.3$ according to the cross-validation results. The performance of the selected SVM classifier was then quantified based on its sensitivity, specificity and the overall accuracy on the test samples (those samples which helped-out during training).

Performance Measurement

To evaluate classifier's performance, we used sensitivity, specificity and accuracy on a per-pixel basis. All measures can be calculated based on four values, namely True Positive (TP, the number of exudates pixels that were correctly detected), False Positive (FP, the number of non-exudates pixels that were wrongly detected as exudates pixels), False Negative (FN, the number of exudates pixels which were not detected), and True Negative (TN, the number of non-exudates pixels that were correctly identified as non-exudates pixels). These values are defined in Table 2.

Table 2. Pixel Based Evaluation

Disease Status			
True Class	Yes	No	Total
Yes	TP	FN	TP+FN
No	FP	TN	FP+TN
Total	TP+FP	FN+TN	TP+FN+FP+TN

From these quantities, the sensitivity, specificity and accuracy computed using Eq. (8), (9) and (10) respectively. Thus "Sensitivity" was defined as percentage of exudates pixels correctly identified, and "Specificity" was defined as percentage of non-exudates pixels correctly identified as non-exudates pixels. Also, "Accuracy" was defined as overall per-pixel success rate of the algorithms.

$$\text{Sensitivity} = \frac{TP}{TP + FN} \tag{8}$$

$$\text{Specificity} = \frac{TN}{TN + FP} \tag{9}$$

$$\text{Accuracy} = \frac{TP + TN}{TP + FP + FN + TN} \tag{10}$$

Results

We performed preprocessing on all 120 training and test images using Matlab. For the optic disc, we used a combination of mathematical morphology method and Otsu's algorithm for optic disc localization. The proposed method achieved a success rate of 97.61% (i.e., the OD was identified correctly in 41 out of the 42 images contained in the local dataset). Each image took approximately 34 seconds to process and localize the OD)

In our experiment, the classification was pixel-based, so each training or test sample represented one pixel in the training or testing image. For each image in the training set, we computed the features for every exudates pixel then randomly selected and computed features from an equal number of non-exudates pixels. The two sets of examples formed our training set. We thus obtained 50,323 examples of exudates pixels and 45,924 examples of non-exudates pixels, for training. From our test images, we used the 21,567 exudates pixels and 19,682 non-exudates pixels as a testing set. The SVM classifier achieved a sensitivity and specificity for the detection of

exudates of 94.46% and 89.52%, respectively. The overall accuracy was 92.14%. Examples of exudates regions predicted by the support vector machine for four test set image are shown in Figure 5. Comparisons between the predicted exudates regions and the corresponding ground truth image are shown in Figure 6.

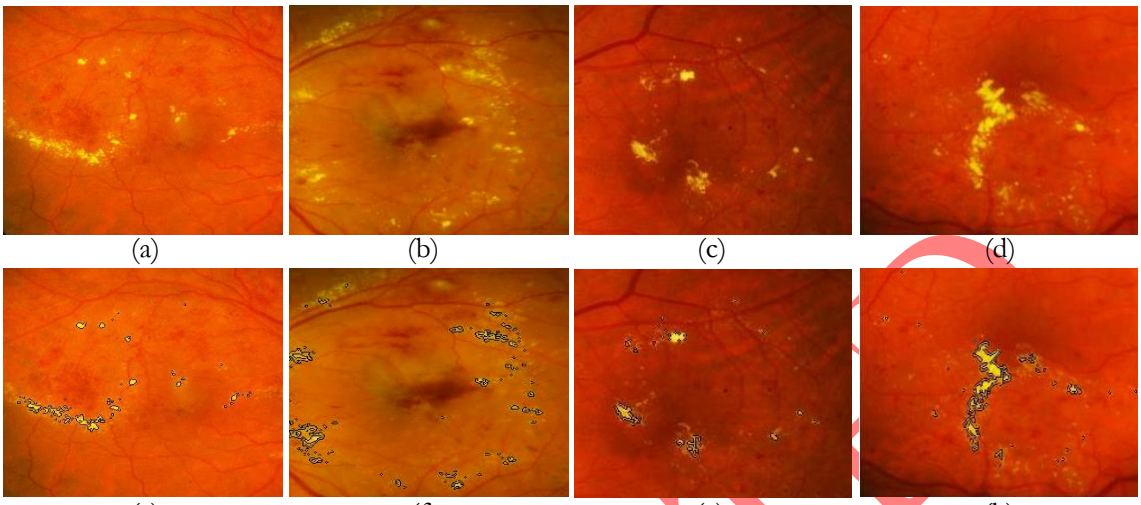

Figure 5 Detection of exudates by the support vector machine classifier. (**a-d**) Four original test set images. (**e-h**) Perimeters of the exudates regions predicted by the support vector machine, superimposed on images (**a-d**)

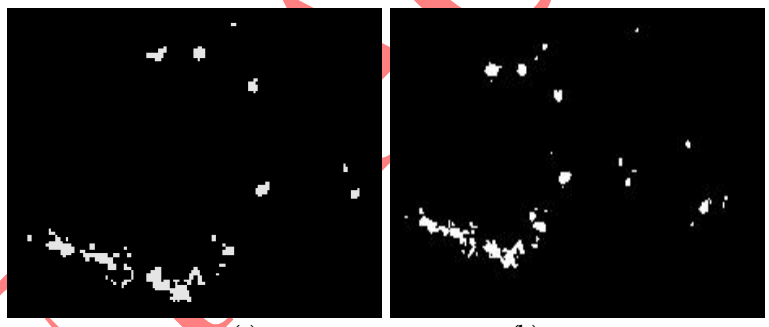

Figure 6 Comparison of support vector machine classifier prediction and ground truth image. (**a**) Exudates pixels predicted by the support vector machine for the original images from Figures 4(**a**). (**b**) Ground truth image for the same images.

Comparative Study

According to experimental results, a fair comparison of our results against the other work is difficult. There is another difficulty in carrying out other people's algorithms due to lack of necessary details. Thus, to evaluate the accuracy of our method, we define two necessary assessment criteria, i.e., sensitivity and specificity. Here, we compare our results with the related works in the literature. These are the works of Zang et al. [1], Wang et al. [11], Osareh [12] and Garcia et al. [13]. A comparison results with other literature is shown in Table 3.

Table 3. Comparison results with other literature (value as %)

Authors	Methods	NI / NIEx	Sensitivity	Specificity
Zang et al. [1]	SVM	213 / 213	88.00	84.00
Wang et al. [11]	SVM	154 / 54	100	71.00
Osareh [12]	FCMC	300 / 300	96.00	94.60
Garcia et al. [13]	Multi Layer Perceptron	50 / 25	84.40	62.70
Our result	SVM	120 / 98	94.46	89.52

Note: NI denoted, the number of retinal image and NIEx denoted the number of retinal image with exudates

Conclusions

In this paper, we developed an automatically decision support application for the purpose of detecting exudates in retinal images. We proposed six features as potential indicators of exudates. We used support vector machine classifiers for feature selection and pixel classification. We used normalized images, enhanced image contrast, filtered images for noise, color space selection and removed the optic disc, then classified those feature using a model built from a training set. The support vector machine classifiers achieved 94.46% for an overall per-pixel sensitivity, specificity of 89.52% and 92.14% for an overall accuracy. This shows that the method can perform in terms of qualitative accuracy, since false detections near true exudates boundaries are qualitatively less serious than isolated false detections. Similarly, a group of false negatives along the boundary of true exudates is qualitatively less serious than a completely missed exudates region. In principle, we could define a new performance measure that weighs false detections and false negatives differently depending on their distance from or connectedness to true exudates regions. This could quantify the performance of the SVM-based classifier. However, in our paper we simply used the standard performance measures and showed the qualitative difference in the investigated images.

Overall, our experimental results showed that careful preprocessing, following with good feature selection, and an appropriate classifier, together, provide excellent detection of exudates performance even on poor retinal images. This clinical application intends to help ophthamologists during exudates screenings to detect symptoms faster and more easily. This is not a final result application but it can be a preliminary diagnosis tool or decision support application for expert ophthalmologists.

Conflict of Interest

The authors declare that they have no conflict of interest.

Acknowledgements

This research was supported by the Commission on Higher Education, Mahasahakham University and King Mongkut's Institute of Technology Ladkrabang. We also would like to thank Mahasarakham Hospital for the images used in this experiment.

References

1. Zhang X, Chutatape O. Top-down and bottom-up strategies in lesion detection of background diabetic retinopathy. Proceedings of the 20-25 Jun. 2005 IEEE Computer Society Conference

on Computer Vision and Pattern Recognition. IEEE Computer Society 2005;2:422-8.
2. Walter T, Klevin JC, Massin P. A contribution of image processing to the diagnosis of diabetic retinopathy detection of exudate in color fundus images of the human retina. IEEE Trans Med Imaging 2002:1236-43.
3. Gardner GG, Keating D, Williamson TH, Elliott AT. Automatic detection of diabetic retinopathy using an artificial neural network: A screening tool. Br J Ophthalmol 1996;80:940-4.
4. Vanrell M, Lumbreras F, Pujol A, Baldrich R, Llados J, Villanueva JJ. Colour normalisation based on background information. International Conference on Image Processing 2001:1111-27.
5. Finlaysona G, Steven H, Gerald S, Yun Tian G. Illuminant and device invariant colour using histogram equalization. Pattern Recognit 2004:179-90.
6. Osareh A, Mirmehdi M, Thomas B, Markham R. Classification and localization of diabetic-related Eye Disease," Proceeding of the 7th European Conference on Computer Vision 2002:502-16.
7. Chang CD, Rong Wu W, Image contrast enhancement based on a histogram transformation of local standard deviation. IEEE Trans Med Imaging 1998;17:518-31.
8. Sangwine S, Horne R. The Colour Image Processing Handbook. Chapman and Hall, 1998.
9. Fukunaga K. Introduction to Statistical Pattern Recognition. Second Edition (Computer Science & Scientific Computing). Academic Press 1990; ISBN: 0-12-269851-7.
10. Osareh A. Comparative exudate classification using support vector machines and neural networks. In Proceeding of the 5th International Conference on Medical Image Computing and Computer-Assisted Intervention-Part II, Springer-Verlag, London, UK 2002:413-20.
11. Wang H, Hsu W, Goh HG, Lee ML. An effective approach to detect lesions in color retinal images. In Proceeding of the IEEE Computer Society Conference on Computer Vision and Pattern Recognition 2000:181-6.
12. Osareh A, Mirmehdi M, Thomas B, Markham R. Classification and localization of diabetic related eye disease. In Proceeding of the 7th European Conference on Computer Vision 2002:502-16.
13. Garcia M, Hormero R, Sanchez C, Lopez M, Diez A. Feature extraction and selection for automatic detection of hard exudate in retinal images. IEEE Conference for Engineering in Medicine and Biology Society 2007:4969-72.